Bioactive Materials 37 (2024) 315–330

Contents lists available at ScienceDirect

Bioactive Materials

journal homepage: www.keaipublishing.com/en/journals/bioactive-materials

# A scaffold vaccine to promote tumor antigen cross-presentation *via* sustained toll-like receptor-2 (TLR2) activation

Daping Xie [a,1], Congwei Han [a,b,1], Chonghao Chen [a], Zhencheng Liao [a], Senio Campos de Souza [a], Yiming Niu [a], João F. Mano [c], Lei Dong [b,d,g,**], Chunming Wang [a,e,f,*]

[a] State Key Laboratory of Quality Research in Chinese Medicine, Institute of Chinese Medical Sciences, University of Macau, Taipa, Macau SAR, China
[b] State Key Laboratory of Pharmaceutical Biotechnology, School of Life Sciences, Nanjing University, Nanjing, 210093, China
[c] Department of Chemistry, CICECO – Aveiro Institute of Materials, University of Aveiro, Campus Universitário de Santiago, 3810-193, Aveiro, Portugal
[d] National Resource Center for Mutant Mice, Nanjing, 210093, China
[e] Department of Pharmaceutical Sciences, Faculty of Health Science, University of Macau, Taipa, Macau SAR, China
[f] Zhuhai UM Science and Technology Research Institute (ZUMRI), University of Macau, Hengqin, China
[g] Chemistry and Biomedicine Innovative Center, Nanjing University, Nanjing, Jiangsu, 210023, China

ARTICLE INFO

*Keywords:*
Scaffold vaccine
TLR2 agonist
Polysaccharide
Reactive oxygen species
Cross-presentation

ABSTRACT

Cancer vaccination holds great promise for cancer treatment, but its effectiveness is hindered by suboptimal activation of $CD8^+$ cytotoxic T lymphocytes, which are potent effectors to mediate anti-tumor immune responses. A possible solution is to switch antigen-presenting cells to present tumor antigens *via* the major histocompatibility complex class I (MHC-I) to $CD8^+$ T cells – a process known as cross-presentation. To achieve this goal, we develop a three-dimensional (3D) scaffold vaccine to promote antigen cross-presentation by persisted toll-like receptor-2 (TLR2) activation after one injection. This vaccine comprises polysaccharide frameworks that "hook" TLR2 agonist (acGM) *via* tunable hydrophobic interactions and forms a 3D macroporous scaffold *via* click chemistry upon subcutaneous injection. Its retention-and-release of acGM enables sustained TLR2 activation in abundantly recruited dendritic cells *in situ*, inducing intracellular production of reactive oxygen species (ROS) in optimal kinetics that crucially promotes efficient antigen cross-presentation. The scaffold loaded with model antigen ovalbumin (OVA) or tumor specific antigen can generate potent immune responses against lung metastasis in B16-OVA-innoculated wild-type mice or spontaneous colorectal cancer in transgenic $Apc^{Min/+}$ mice, respectively. Notably, it requires neither additional adjuvants nor external stimulation to function and can be adjusted to accommodate different antigens. The developed scaffold vaccine may represent a new, competent tool for next-generation personalized cancer vaccination.

## 1. Introduction

Cancer vaccination, aimed at inducing the body's adaptive immunity against tumor antigens, holds great promise in cancer treatment [1,2]. A common challenge for its clinical application is inadequate activation of immune responses mediated by cytotoxic T cells ($CD8^+$), which are the most potent effectors [3]. Tumor antigens in the vaccine should be presented by the major histocompatibility complex class I (MHC-I) molecules on the antigen-presenting cells (APCs), primarily dendritic cells (DCs), to $CD8^+$ T cells – a process known as cross-presentation [4]. However, upon taken by APCs, these antigens are typically degraded within the endosome-lysosome compartment and unable to undergo MHC-I presentation [5], unless they can escape from the endosomal compartment and be swiftly transported to the cytosol [6].

Increasing evidence has shown that elevated production of intracellular reactive oxygen species (ROS) facilitates this escaping process. ROS maintain active alkalinization of the phagosomal lumen to suppress lysosomal proteases with low pH optima [7] and oxidize the lipids on the

Peer review under responsibility of KeAi Communications Co., Ltd.
* Corresponding author. State Key Laboratory of Quality Research in Chinese Medicine, Institute of Chinese Medical Sciences, University of Macau, Taipa, Macau SAR, China.
** Corresponding author. State Key Laboratory of Pharmaceutical Biotechnology, School of Life Sciences, Nanjing University, Nanjing, 210093, China.
*E-mail addresses:* leidong@nju.edu.cn (L. Dong), cmwang@umac.mo (C. Wang).
[1] Equal contribution.

https://doi.org/10.1016/j.bioactmat.2024.03.035
Received 7 January 2024; Received in revised form 28 March 2024; Accepted 29 March 2024

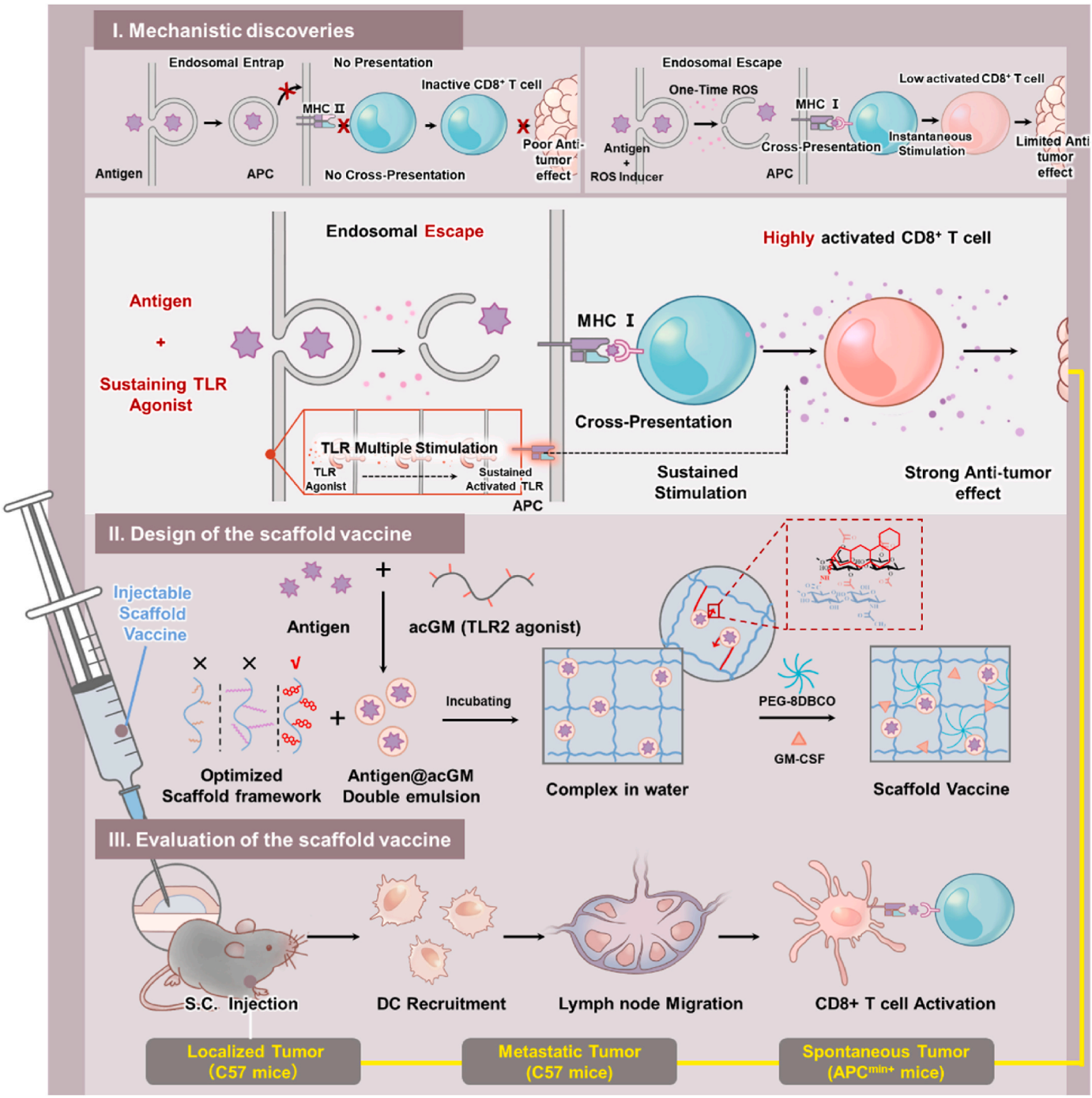


**Scheme 1. Schematic illustration of the scaffold vaccine that promotes antigen cross-presentation to trigger anti-tumor immune responses**. To create optimal intracellular ROS kinetics for lysosomal disruption and antigen escape (as discovered in this study), a 3D injectable scaffold is designed for the "retention-and-release" of a TLR2 agonist glycan upon subcutaneous implantation. Installation of tunable hydrophobic interactions between the scaffold and the "hooked" agonist enables sustained TLR activation in the abundantly recruited DCs *in situ*, which triggers consequently efficient cross-presentation of tumor antigens. The efficacy of this novel scaffold vaccine is subsequently undergoing comprehensive evaluations in both wild-type and transgenic mice against localized, metastatic, and spontaneous tumors.

endosomal membrane to aid antigen leakage into the cytosol [8] for cross-presentation. Accordingly, researchers deliver small-molecule compounds [9,10] or stimuli-responsive biomaterials (e.g. nanozymes [11] or photosensitizers [12]) to trigger intracellular ROS production. Nevertheless, despite these inspirational designs, three key challenges remained. First, to initiate optimal cross-presentation, only APCs are expected to produce more ROS; but the ROS-triggering methods have no selectivity and can affect other cell types, causing potential safety concerns [13]. Second, in addition to triggering MHC-I antigen presentation, an immunostimulatory microenvironment needs to be shaped to enhance $CD8^+$ T cell activation, including the secretion of proper pro-inflammatory cytokines [14] and upregulation of CD80/86 in APCs [15,16] – a demand that current ROS-inducing methods either do not focus on or require extra components (e.g. adjuvants [17]) to fulfil. Third, the kinetics of ROS production (e.g., level and duration) is crucial, since its burst or excessive intracellular accumulation is cytotoxic [18].

To overcome these challenges, we proposed modulating cell-surface toll-like receptors (TLRs) to enhance cross-presentation. First, TLRs belong to pattern recognition receptors (PRRs) preferentially expressed by macrophages and DCs to recognize danger signals [19]; thus, modulating TLRs enables targeting a selective and desirable range of cells, e.g. DCs. Next, their activation induces both intracellular ROS production [20] and pro-inflammatory cytokines that strengthen $CD8^+$ T cell activation [21–23] – hence targeting the two key criteria for cross-presentation, without requiring additional adjuvants or external triggering. Thus, activating TLRs on DCs for antigen escaping, with a clear and intrinsic biological mechanism, is potentially efficient and controllable to facilitate cross-presentation. However, TLR activation is instantaneous [24]; one-time activation might not produce sufficient intracellular ROS required for aiding antigen escaping, while excessive TLR stimulation could be harmful. Therefore, the focus of this work is how to activate TLRs to induce intracellular ROS production in optimal kinetics that favors antigen cross-presentation.

To realize this goal, in this study, we aimed to devise a three-dimensional (3D) injectable scaffold vaccine enabling sustained TLR2 activation in DCs to promote antigen cross-presentation and eventually induce lasting anti-tumor immune responses. We synthesized a polysaccharide-based 3D scaffold decorated with optimized hydrophobic moieties, which could "hook" an amphiphilic TLR2 agonist – an acetyl glucomannan (acGM) polysaccharide [25,26] – within the scaffold. The retention and release of acGM from this scaffold enabled sustained TLR2 stimulation to induce cross-presentation. We postulated that this scaffold vaccine, loaded with tumor antigens and acGM, could recruit and educate abundant DCs to produce intracellular ROS in optimal kinetics, leading to adequate cross-presentation and robust $CD8^+$ T cell-mediated immunity, as further validated in a lung metastatic model in wild-type mice and spontaneous tumor model in transgenic mice ($Apc^{Min/+}$) (Scheme 1).

## 2. Materials and methods

### 2.1. Chemicals and reagents

Ovalbumin was purchased from Sigma-Aldrich (USA). $Pam_3CSK_4$ and Poly (I:C) were purchased from Invitrogen (USA). Fetal bovine serum, the cell culture media of RPMI 1640 and DMEM, and penicillin-streptomycin (100 × ) were purchased from Gibco-Thermo Fisher (USA). PE/Cyanine7 anti-mouse CD11c antibody, PE anti mouse CD86 antibody and other flow cytometry antibodies are purchased from Biolegend (USA). Glucomannan (GM) from Konjac was purchased from Shimizu Chemical Corporation (Japan). The 8-arm PEG amine and PEG-8DBCO were purchased from Ponsure (Shanghai, China). diSulfo-Cy5 DBCO (Methyl) were purchased from Confluore Biological Technology (China). Hyaluronic acid with a molecular weight of 800 kDa to 1 MDa, 1-Tetradecylamine, n-hexylamine and other chemicals were purchased from Aladdin (Shanghai, China), unless otherwise indicated.

### 2.2. Cell and animals

The detailed ethics information is provided in the 'Ethics Approval' section. B16–F10-OVA (designated as B16-OVA) was purchased from Shanghai Fuheng Biotechnology Co., Ltd. DC2.4 cell was purchased from the American Type Culture Collection (ATCC, USA). Bone marrow-derived dendritic cells (BMDCs) were isolated from 6 to 8 weeks C57BL/6J mice and cultured in RPMI 1640 medium supplemented with 10% inactivated fetal bovine serum and 1% penicillin-streptomycin. GM-CSF (20 ng/mL) and IL4 (10 ng/mL) were used for BMDCs differentiation. B16-OVA tumor cells were maintained in a 5% $CO_2$ environment with Dulbecco's modified Eagle's medium (DMEM) supplemented with 10% FBS and L-glutamine (2 mM).

### 2.3. Synthesis and characterization of acGM

Acetyl glucomannan (acGM) was synthesized as previously reported by our group [25] from low molecular weight GM (~8 kDa). Briefly, GM (1.0 g) was dissolved in 50 mL DMF stirred at 50°C for 1 h and then added with acetic anhydride (5.25 mL, 3 equivalent) and pyridine (4.591 mL, 3 equivalent). After 10 h, the mixture was poured into dd-$H_2O$ (100 mL), and acGM was extracted by dichloromethane. The extraction was washed twice with HCl (1 M, 100 mL) and dd-$H_2O$ (100 mL) to remove the residual pyridine. acGM with a degree of substitution (DS) of 1.8 was obtained by evaporation as a white powder.

### 2.4. Preparation of OVA@acGM and TSA@acGM

acGM (100 mg) was dissolved in 1 mL dichloromethane, added with 100 μL PBS or PBS containing OVA (5 mg) or tumor lysate (100 μL, 50 mg/mL). This mixture was emulsified through sonication for 30 s on ice using a probe sonicator with an output of 20%. Then, the primary emulsion was added to PVA solution (3%, 2 mL) and emulsified for a further 1 min. The W/O/W was transferred to PVA solution (0.3%, 20 mL) and stirred to evaporate the dichloromethane. The nanoparticles were collected *via* centrifugation at a speed of 15,000 rpm for 15 min, re-suspended in dd-$H_2O$ (2 mL), and finally lyophilized. The morphology of OVA@acGM was characterized by scanning electron microscopy (SEM) with a S-5000 microscope after sputter coating with a palladium/gold alloy. Particles were suspended in dd-$H_2O$ at 2 mg/mL. Particle size distributions and zeta potential were determined by dynamic light scattering (Zetasizer, Malvern Instruments).

For the spontaneous tumor model, the tumor was digested by DNAase-I and Collagenase-IV. the tumor-specific antigen (TSA) was extracted by 3 freeze-thaw cycles in liquid nitrogen and 37°C water baths. The whole cell suspension was sonicated in an ice bath, followed by centrifugation at 600*g* for 10 min. The supernatant was collected and centrifuged at 13500 g for 10 min. The obtained supernatant was obtained and quantified by a BCA protein assay kit. The TSA was incorporated into acGM by double emulsion.

### 2.5. Synthesis of $N_3$-HA-C6, $N_3$-HA-C14, and $N_3$-HA-DOCA

Hyaluronic acid (HA) was first converted to $N_3$-HA. Briefly, HA (1 g, ~10 kDa, 1 eq.) was dissolved in MES solution (50 mL, 0.1 M, pH 5.5). EDC•HCl (959 mg, 2 eq.) and NHS (719 mg, 2.5 eq.) were added to activate the carboxyl group of the HA. After 30 min, 3-Azido-1-propanamine (125 mg, 0.5 eq.) was added and stirred overnight. The $N_3$-HA was obtained by dialysis (MWCO 5 kDa) against dd-$H_2O$ and lyophilization. The DS of azide group was 0.07.

To further modify the $N_3$-HA with hydrophobic moieties, the prepared $N_3$-HA (1 g, 1 eq.) was dissolved in a mixed solution (DMSO/MES buffer = 1:1, v/v). EDC•HCl (923 mg, 2 eq.) and 692 mg NHS were added to activate the carboxyl group of the $N_3$-HA. After 30 min, n-hexylamine (50 mg, 1 eq.) was added and stirred at room temperature overnight. The $N_3$-HA-C6 was obtained by dialysis against dd-$H_2O$ for 48 h. $N_3$-HA-DOCA or $N_3$-HA-C14 was synthesized using the same method with slight modifications. As both tetradecylamine and DOCA-$NH_2$ were solid, the solution was centrifuged and filtered to remove the residuals. The final products were obtained by lyophilization and characterized by $^1$H NMR and FTIR.

### 2.6. Cross-linking of the scaffold vaccine

The scaffold vaccine was cross-linked by click reaction. $N_3$-HA or its derivates (2 mg) was dissolved in 50 μL PBS containing GM-CSF (5 μg) and OVA@acGM (50 μg). Sonication was used to disperse the OVA@acGM in the solution. Then, PEG-8DBCO (50 μL, 2 mg) was added to crosslink HA derivates containing azide moieties through a click reaction.

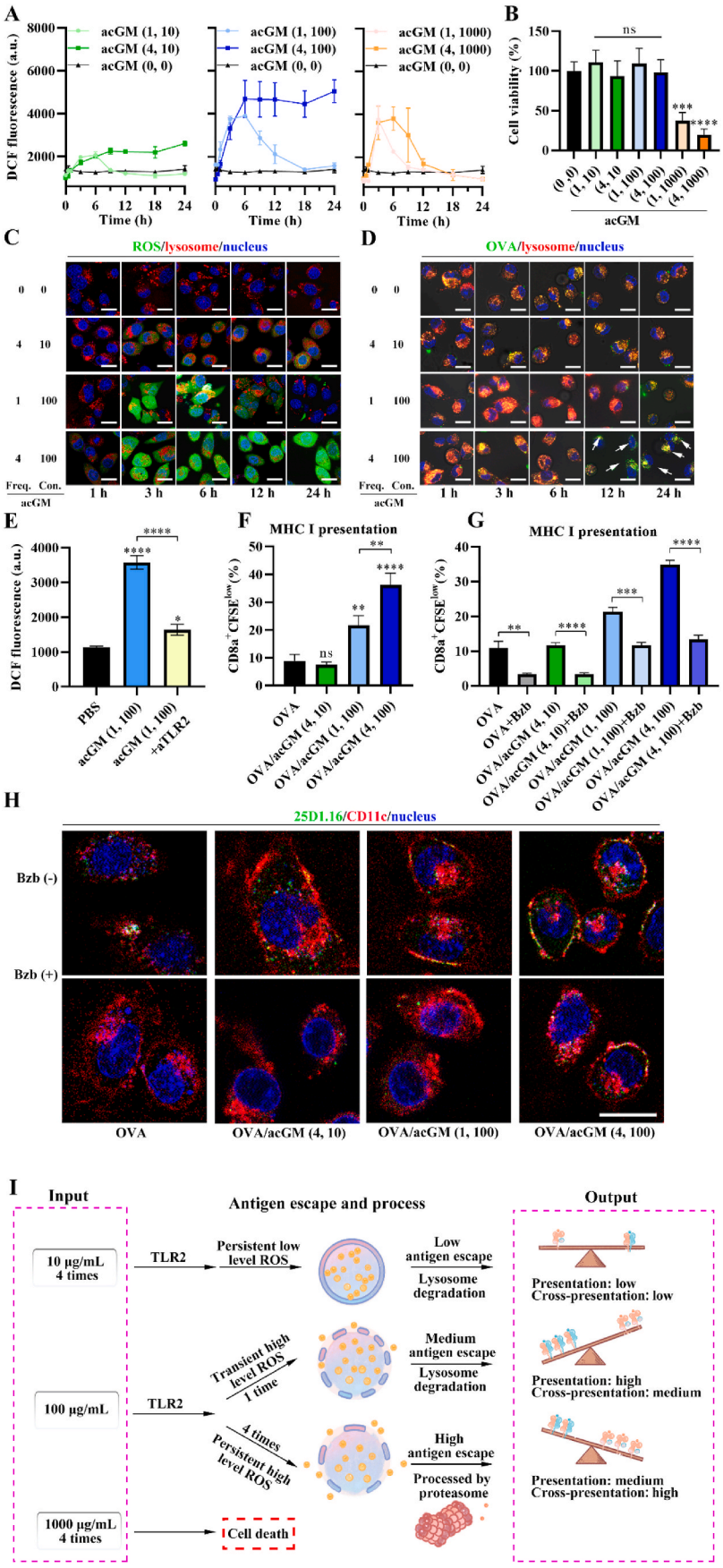


(caption on next page)

**Fig. 1.** The effect of intracellular ROS kinetics on the mode of antigen presentation. (A) ROS kinetics in BMDCs induced by acGM at different concentrations and frequencies. Left panel: 10 μg/mL acGM; Middle panel: 100 μg/mL acGM; Right panel: 1000 μg/mL acGM. **(B)** Cell viability of BMDCs following acGM treatment at different concentrations and frequencies. **(C)** The lysosome disruption caused by ROS. Lysosomes were stained with Lyso-Tracker (red). Nuclei were stained with Hoechst 33342 (blue). ROS signal was green. Scale bar: 20 μm. Freq.: frequency; Con.: concentration. **(D)** Antigen escapes from lysosomes. Lysosomes were stained with Lyso-Tracker (red). Nuclei were stained with Hoechst 33342 (blue). OVA were labeled with FITC (green). Scale bar: 20 μm. Freq.: frequency; Con.: concentration. **(E)** ROS induction through TLR2 activation. **(F)** MHC-I antigen presentation of OVA/acGM (4, 100). BMDCs were pulsed with OVA (50 μg/mL) for 15 min and then treated with acGM, followed by co-culturing with CFSE-labeled, OVA-specific $CD8^+$ or $CD4^+$ T cells for 48 h as described in **Materials and Methods**. MHC-I and MHC-II antigen presentation were determined by measuring DC-primed $CD8^+$ and $CD4^+$ T cell proliferation (defined as $CFSE^{low}$), respectively. **(G)** MHC-I antigen presentation pre-treated by bortezomib (Bzb), a proteasome inhibitor. **(H)** Confocal image of BMDC treated with OVA/acGM (X, Y) or Bzb + OVA/acGM (X, Y). Green signal showed the expression of 25D1.16. Red signal showed the expression of CD11c. Nuclei were stained with Hoechst 33342 (blue). Scale bar: 20 μm. **(I)** The effect of TLR2 activation-induced ROS kinetics on lysosome disruption and antigen processing. $n = 3$, values represent means ± standard deviation. Statistical significance was calculated by one-way ANOVA using the Tukey posttest. ns: no significance; $^*p < 0.05$, $^{**}p < 0.01$, $^{***}p < 0.001$, $^{****}p < 0.0001$.

### 2.7. In vitro activation of BMDCs

The GM-CSF and IL-4-treated BMDCs were harvested on day 7. The BMDCs were incubated with acGM (100 μg/ml) for 24 h. The supernatant was discarded, and the co-stimulatory molecules were detected by flow cytometry. CD11c was used as the marker of BMDCs; CD80, CD86, MHC-II, and CD40 were used as the markers of mature BMDCs.

### 2.8. Antigen presentation

MHC-I and II antigen presentation of BMDCs was determined by assessing DC-primed $CD8^+$ and $CD4^+$ T cell proliferation. Briefly, BMDCs were treated with acGM at different concentrations and frequencies. To obtain OVA-specific T cells, C57BL/6J mice were immunized with 20 μg OVA and 20 μg Poly I:C (InvivoGen, CA, USA) by intraperitoneal injection once per week for three weeks. After the final immunization, splenic $CD8^+$ and $CD4^+$ T cells were purified using the specific cell isolation kit (Miltenyi Biotec, CA, USA).

To determine MHC-I antigen presentation of DCs, $CD8^+$ and $CD4^+$ T cells were pre-labeled with 5, 6-carboxyfluorescein diacetate succinimidyl ester (CFSE) and co-cultured with OVA-loaded DCs (pre-treated without Bzb or with Bzb) at the ratio of T cells to DCs at 10:1 at 37 °C for 48 h. The proliferation of $CD8^+$ and $CD4^+$ T cells, representing the MHC-I and MHC-II antigen presentation by BMDCs, respectively, was determined by measuring the live cells with decreased CFSE intensity ($CFSE^{low}$ cells).

### 2.9. Biodistribution in vivo

To investigate the retention of the scaffold, the HA derivates were labeled with Cy5 before crosslinking *via* click chemistry. The scaffold vaccine was cross-linked and injected into the flank of the mice. At indicated time points, the signal of the scaffold was monitored by IVIS. To investigate the retention of acGM, acGM was labeled with Cy5 before encapsulating OVA. The Cy5-labeled OVA@acGM were formulated into the scaffold vaccine. Then, the scaffold vaccine was injected into the flank of the mice. The signal of the scaffold was monitored by IVIS at indicated time points.

### 2.10. In vivo dendritic-cell migration, activation, and ROS detection assays

$N_3$-HA-DOCA or $N_3$-HA were incubated with OVA@acGM overnight under sonication. Then, PEG-8DBCO containing GM-CSF was added to form the injectable scaffold vaccine. The scaffold vaccine was injected subcutaneously into the left flank of 6-8-week-old female C57BL/6J mice (100 μL each mouse). To analyze DC recruitment, the isolated cells were stained with primary antibodies (Biolegend, CA, USA) conjugated to fluorescent markers for flow cytometric analysis. For ROS detection, the cells were incubated with DCFH-DA for 30 min and detected immediately by flow cytometry. For histological examination, scaffolds were cut, paraffin-embedded, and stained with hematoxylin and eosin (H&E).

### 2.11. Tumor growth assays and T cell responses

The scaffold vaccine was injected subcutaneously into the left flank of 6-8-week-old female C57BL/6J mice (100 μL/each mouse). Animals were challenged 7 days later with a subcutaneous injection of $1 \times 10^6$ B16-OVA cells into the right flank. Animals were monitored for the onset of tumor growth (approximately 1 $mm^3$) and euthanized when a tumor reached 1500 $mm^3$. To evaluate T lymphocyte infiltration, B16-OVA melanomas were dissected and prepared into single-cell suspensions at 18 d post-tumor inoculation. The cells were stained with FITC anti-mouse CD3, PE anti-CD4 and APC anti-mouse CD8, and then measured by flow cytometry. Meanwhile, tumor tissues were prepared into paraffin sections and analyzed *via* multiplex immunohistochemistry staining. The slices were examined under a DMI8 microscope.

For the spontaneous model, the scaffold vaccine was injected subcutaneously into the left flank of 8-week-old $Apc^{Min/+}$ mice. These mice were given water with 2.5% sodium dextran sulfate (DSS) for one week and then transitioned to a regular water supply but on a high-fat diet (constituting 60% of their calorie intake). Upon observing the presence of blood in their stool, the mice were humanely euthanized. Subsequently, their colons were harvested, and the count of polyps in the colon tissue was determined. The cells were stained with FITC anti-mouse CD3, PE anti-CD4, APC anti-mouse CD8, and then measured by flow cytometry. Meanwhile, tumor tissues were prepared into paraffin sections and analyzed *via* multiplex immunohistochemistry staining. The slices were stained with anti-mouse CD8, anti-mouse IFN-γ and anti-mouse GramB, followed by staining with corresponding secondary antibodies. The slices were examined under a DMI8 microscope.

### 2.12. Statistical analysis

Data for all experiments were recorded using Excel and analyzed using Prism Software. All numerical values are presented as mean ± standard deviation (SD). Statistical significance was calculated using a one-way ANOVA with Tukey's post hoc test for multiple comparisons or a two-tailed *t*-test for two comparisons. A significance level of 0.05 was used to determine statistically significant differences between groups.

## 3. Results

### 3.1. Assessment of intracellular ROS kinetics for antigen cross-presentation

The TLR2-activating polysaccharide acGM was prepared as previously reported [25], with a particle size of ~210.0 ± 7.7 nm (Fig. S1A). Its activation of BMDCs was validated by flow cytometry, with an increased expression of CD80, CD86, MHC-II, and CD40 (Figs. S1B–C). To test the effect of acGM-triggered TLR2 activation on ROS production, BMDCs were treated by acGM in the ways described as acGM (X, Y) – at different frequencies (X: 1 time or 4 times) and concentrations (Y: 10, 100, or 1000 μg/mL) and monitored by flow cytometry following DCFH-DA staining.

As shown in Fig. 1A and Fig. S2, one-time treatment by acGM or

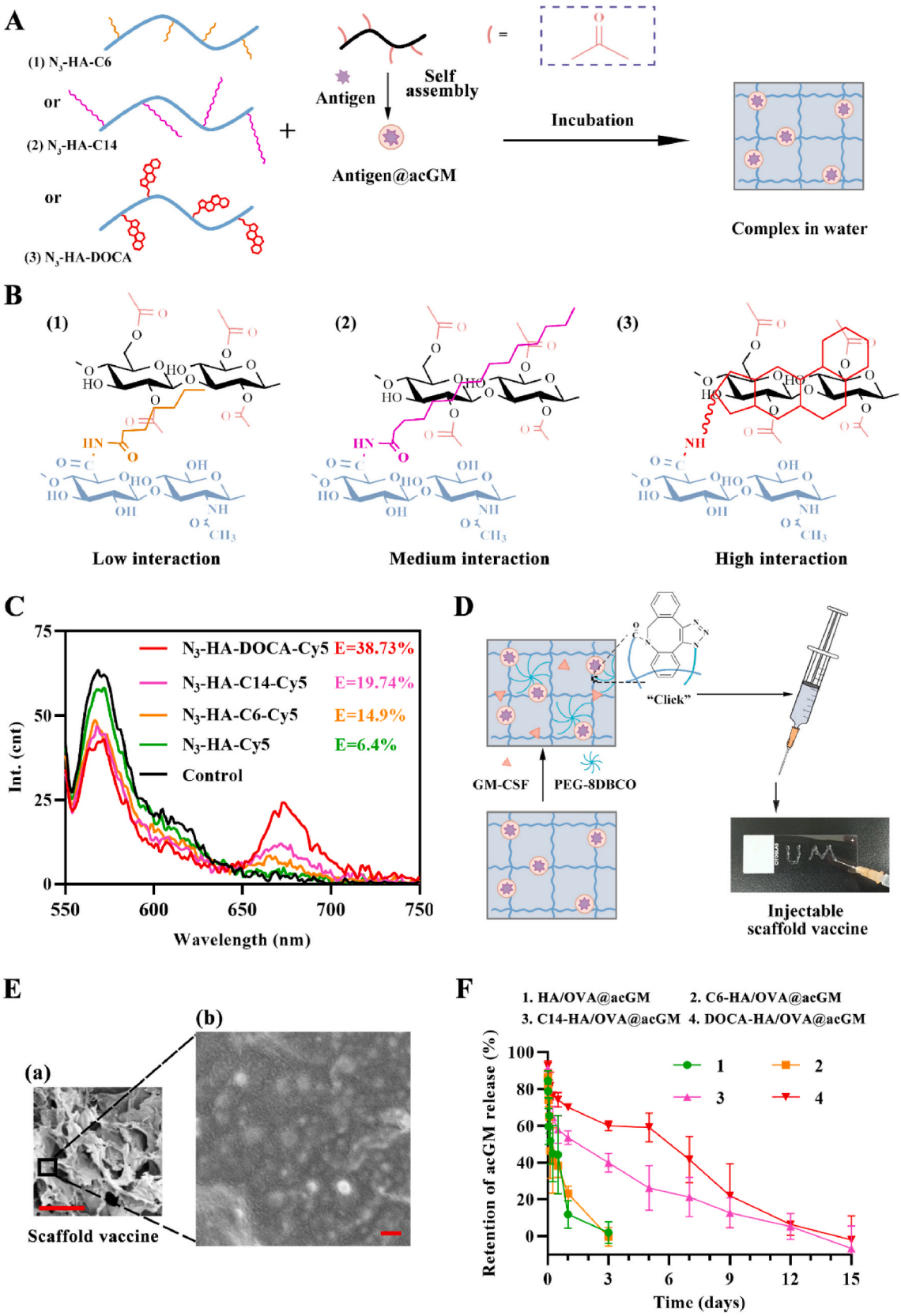


**Fig. 2.** Design of the injectable, 3D scaffold vaccine for acGM "retention-and-release" *in situ* upon subcutaneous implantation. (A) Schematic illustration of hydrophobic modification of hyaluronic acid to enhance its interaction with acGM. **(B)** Interactions between HA derivatives and acGM. **(C)** Representative spectra excited at 550 nm, showing the effect of altering Cy3-Cy5 donor-acceptor spacing in acGM-Cy3 and Cy5 labeled HA derivatives. **(D)** Schematic of preparation of scaffold vaccine based on click chemistry. **(E)** Morphology of DOCA-HA/OVA@acGM. **(F)** Retention of acGM from scaffold vaccine. 1: HA/OVA@acGM; 2: C6-HA/OVA@acGM; 3: C14-HA/OVA@acGM; 4: DOCA-HA/OVA@acGM. $n = 3$, values represent means ± standard deviation. Statistical significance was calculated by one-way ANOVA using the Tukey posttest. ns: no significance; $^{*}p < 0.05$, $^{**}p < 0.01$, $^{***}p < 0.001$, $^{****}p < 0.0001$.

$Pam_3CSK_4$ (a TLR2 agonist) in all concentrations was sufficient to induce ROS production in BMDCs, but repeated stimulations with acGM (4, 100) four times within 24 h led to a high and sustained ROS production. First, one-time stimulation with all acGM concentrations increased ROS to reach a plateau at around 3 h, drop from 6 h (except for acGM (1, 1000) immediately at 3 h), and eventually fall to baseline (non-treatment) after 9–18 h. Second, increasing the acGM dose from 10 to 100 μg/mL could – while further increasing it from 100 to 1000 μg/mL failed to – significantly elevate ROS production. Third, for acGM at 10 and 100 μg/mL, a four-time stimulation within 24 h led to sustained production of ROS over 24 h, despite the level in the latter being double that in the former. The fact that acGM (4, 1000) did not induce sustained ROS production could be attributed to its toxicity at this high concentration to BMDCs, while the other two doses did not affect cell viability (Fig. 1B). These results indicated that both the concentration and treatment frequency of acGM influenced the ROS production in BMDCs.

Next, we investigated the effect of ROS kinetics induced by acGM (4, 10), acGM (1, 100), or acGM (4, 100) on the lysosome disruption. As shown in Fig. 1C and Fig. S3, in the first 6 h, the fluorescence of lysotracker maintained a high level for all groups, while ROS reached a high level in both acGM (1, 100) and acGM (4, 100). For BMDC with a persistently high level of ROS induced by acGM (4, 100), the red fluorescence significantly decreased by 24 h. However, for BMDCs treated with acGM (1, 100), where ROS decreased from 12 h, and those treated with acGM (4, 10), where the ROS maintained at a medium level, the red fluorescence showed no clear decrease. Thus, repeated stimulation by acGM at 100 μg/mL was optimal for inducing sustained ROS production and lysosome disruption.

Then, BMDCs were exposed to OVA (50 μg/mL) for 15 min and immediately treated with acGM to investigate the influence of ROS on antigen escape. As shown in Fig. 1D and Figs. S4–S7, the co-localizations (merged into yellow) of the FITC-OVA green signal were observed mainly in the first 6 h for all groups. Subsequently, OVA was diffused from the lysosomes at 12 and 24 h (Fig. S8) in BMDCs with persistently high-level ROS induced by acGM (4, 100), as indicated by the white arrows, while red fluorescence was weakened. In comparison, BMDCs treated with acGM (1, 100) produced high-level ROS for only 3 h and had less diffusion of green fluorescence, and those treated with acGM (4, 10) showed little diffusion of green fluorescence. This finding suggested that both ROS level and duration time were crucial to facilitate the antigen escape from lysosome. Furthermore, pre-treating the BMDCs with a neutralizing anti-TLR2 antibody significantly weakened ROS production at 6 h by acGM (1, 100) treatment (Fig. 1E), verifying ROS increase as a consequence of TLR2 activation.

Since the lysosome escape of antigen facilitates MHC-I antigen presentation, we evaluated the effect of escaped antigen on MHC-I and MHC-II antigen presentation by measuring DC-primed $CD8^+$ and $CD4^+$ T cell proliferation, respectively. Treated with OVA and acGM likewise, BMDCs were incubated with CFSE-labeled, OVA-specific $CD8^+$ T cell or OVA-specific $CD4^+$ T cells for 2 days. MHC-I and MHC-II antigen presentation were determined by measuring DC-primed $CD8^+$ T cell and $CD4^+$ T cell proliferation. As indicated in Fig. 1F, the MHC-I presentation efficiency of BMDC treated with OVA/acGM (4, 100) was the highest, 4.1 times that of those treated with OVA/acGM (4, 10). Interestingly, for MHC-II presentation, BMDCs treated with OVA/acGM (1, 100) showed the highest efficiency among all groups (Fig. S9A).

Because the activation of cross-presentation by escaped antigens involves proteasomes, we pre-treated the DCs with a proteasome inhibitor (Bortezomib, Bzb) before adding OVA/acGM (X, Y) and observed a significant decrease in the cross-presentation efficiency (Fig. 1G). Similarly, the increased expression of 25D1.16 (MHC-I and $OVA_{257\text{-}264}$ complex) by OVA/acGM (4, 100) was suppressed by proteasome inhibition (Fig. 1H), further highlighting the process of proteasome-involved cross-presentation. The inhibitor itself did not influence antigen presentation (Fig. S9B).

Collectively, the above data suggested that different stimulating patterns by acGM could modulate the modes of antigen presentation, *via* stimulating different ROS kinetics and thereby influencing antigen escape from the lysosome, and confirmed the necessity of repeated TLR activation for initiating effective cross-presentation (Fig. 1I).

### 3.2. Design of scaffold vaccine for acGM retention via hydrophobic interaction

As demonstrated above, ROS kinetics in BMDCs treated with acGM at a concentration of 100 μg/mL for 4 times per 24 h could optimally facilitate antigen escape to promote cross-presentation. Since it is impractical to perform repeated treatment *in vivo*, we devised a scaffold for acGM retention to achieve such kinetics, based on hydrophobic interactions within the gel scaffold formed *via* click chemistry.

We modified hyaluronic acid (HA) with different hydrophobic groups to seek optimal hydrophobic interactions with the hydrophobic moieties of acGM (Fig. 2A). Briefly, the HA was modified with azide group and subsequently with: i) *N*-hexylamine with six carbon (C6), ii) 1-tetradecylamine with fourteen carbon (C14), or iii) Deoxycholic acid derivatized amines (DOCA-$NH_2$) with a large hydrophobic moiety. The hydrophobic moieties were designed to interact with the hydrophobic acGM, as indicated in Fig. 2B. The synthesis route of these HA derivatives was shown in Fig. S10A. The azide groups were reserved for subsequent scaffold preparation. The stretching vibration of the azide group was observed at 2100 $cm^{-1}$, indicating that azide groups were successfully modified to HA (Fig. S10B). The $^1H$ NMR spectrum (Fig. S10C) showed that C6 or C14 chain was modified to the $N_3$-HA, with the chemical shift at 1.28 ppm and 0.86 ppm showing the presence of $–CH_2$- and $–CH_3$, respectively. The peak at the chemical shift of 0.69 ppm was a characteristic peak of $–CH_3$ in the deoxycholic acid (DOCA), indicating that DOCA was successfully modified to the $N_3$-HA.

Then, we evaluated the interaction between the HA-derivatives and acGM using fluorescence resonance energy transfer (FRET). Briefly, acGM labeled with Cy3 was incubated with HA-derivatives labeled with Cy5, and the spectra excited at 550 nm was detected. As shown in Fig. 2C, $N_3$-HA with no hydrophobic groups hardly interacted with acGM, as little FRET phenomenon was observed (FRET efficiency: 6.4%). Among all groups, the FRET efficiency was the highest (38.73%) with the $N_3$-HA-DOCA/acGM mixture, suggesting their relatively strongest interactions. Further, morphological observation of the complexes by SEM confirmed that $N_3$-HA-DOCA formed clearer aggregates than other groups (Fig. S10D), validating that hydrophobic modification could enhance the interaction between HA derivatives and acGM, which is the prerequisite for acGM retention.

Next, we prepared the 3D, injectable scaffold vaccine *via* click chemistry. As shown in Fig. 2D, HA derivatives ($N_3$-HA, $N_3$-HA-C6, $N_3$-HA-C14, $N_3$-HA-DOCA) with azide groups were crosslinked with PEG-8DBCO – in addition to OVA@acGM (Fig. S11A) or TSA@acGM (Fig. S11B) and GM-CSF as standard components for DC recruitment – to fabricate the scaffold by simple mixing. The scaffold vaccine can be injected through a conventional needle (27-gauge) (Fig. 2D). The inset photos illustrated the sol-gel transition of the scaffold (Fig. S12A). As an important feature, this scaffold vaccine possessed a continuous and porous structure under SEM (Fig. 2E–a), with acGM particles dispersed and within the scaffold (Fig. 2E–b). Hydrophobic modification of HA did not affect the mechanical properties of the scaffold (Fig. S12B).

The scaffolds modified with DOCA (DOCA-HA) significantly prolonged acGM release, with over 50% of the amount still retained after 6 days; in comparison, the ones modified with C14 exhibited moderate retention (~21%) while those with C6 failed to "hook" acGM (Fig. 2F). These findings were consistent with the above SEM observation of the complexes, suggesting that the DOCA-HA network could effectively retain and release acGM. In addition, the scaffold and its components exerted no cytotoxicity to DC2.4 and NIH-3T3 cells (Figs. S13 and S14). Hence, DOCA-HA/OVA@acGM and HA/OVA@acGM, with high and no retention of acGM, respectively, were selected for comparison in the

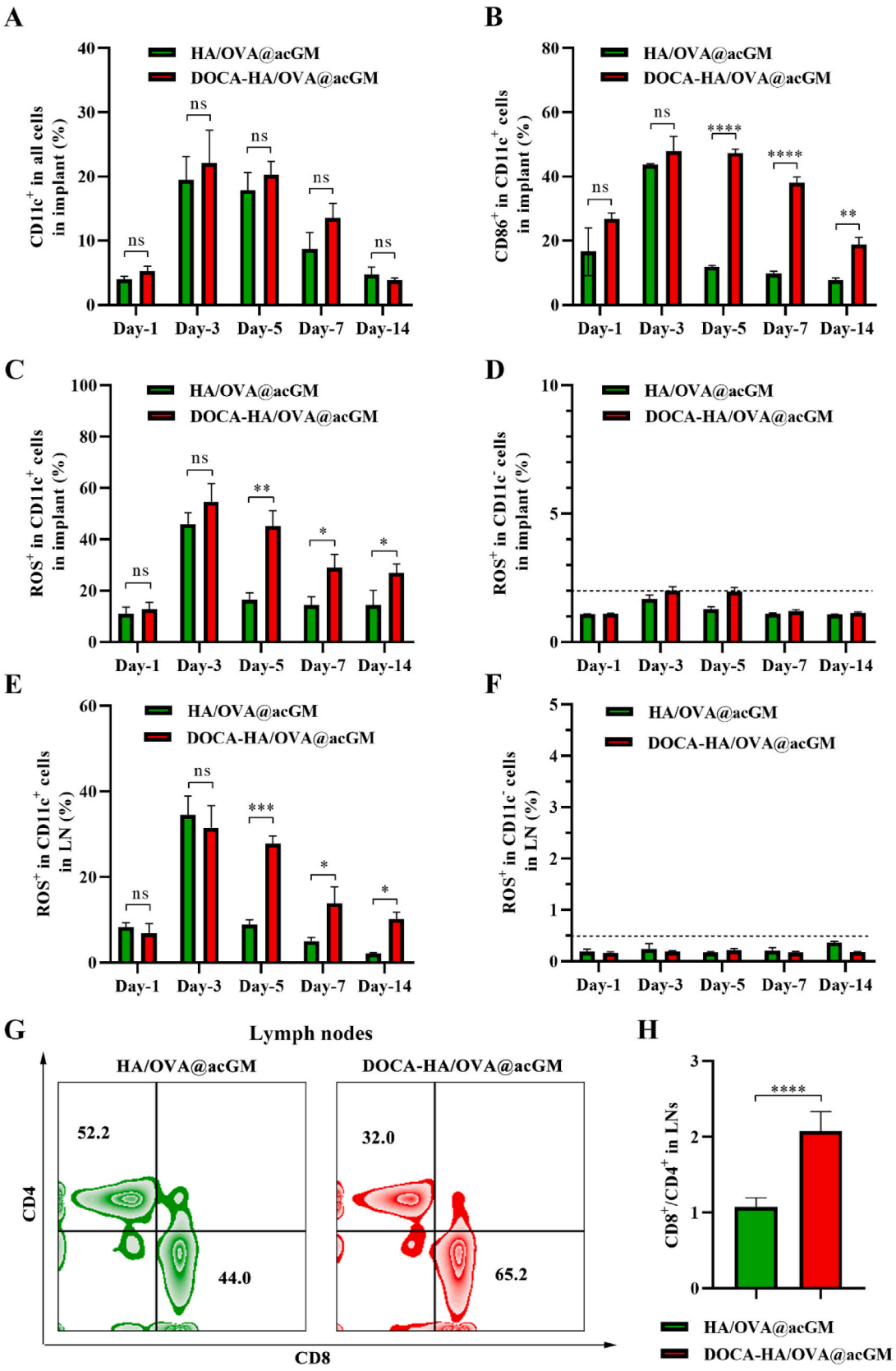


**Fig. 3. The scaffold vaccine promoted DC maturation and ROS production *in vivo*.** **(A)** The number of $CD11c^+$ DCs recruited by HA/OVA@acGM and HA-DOCA/OVA@acGM at indicated time points after injection. **(B)** Maturation of $CD11c^+$ DCs recruited by HA/OVA@acGM and HA-DOCA/OVA@acGM at indicated time points after injection. **(C)** Proportion of $ROS^+$ in $CD11c^+$ cells in implant. **(D)** Proportion of $ROS^+$ in $CD11c^-$ cells in implant. **(E)** Proportion of $ROS^+$ in $CD11c^+$ cells in lymph nodes. **(F)** Proportion of $ROS^+$ in $CD11c^-$ cells in lymph nodes. **(G)** Representative flow cytometry plots of $CD8^+$ T cells and $CD4^+$ T cells in $CD3^+$ T cells in lymph nodes. **(H)** Proportion of $CD8^+$ T cells and $CD4^+$ T cells in $CD3^+$ T cells in lymph nodes. $n = 3$, values represent means ± standard deviation.

Statistical significance was calculated by one-way ANOVA using the Tukey posttest or student's t-test. ns: no significance; *$p < 0.05$, **$p < 0.01$, ***$p < 0.001$, ****$p < 0.0001$.

following experiments *in vivo*.

### 3.3. In vivo assessment of the scaffold vaccine in inducing DC maturation and $CD8^+$ T cell activation

To verify that scaffold vaccine with acGM retention could consistently stimulate TLR2, we perform experiment using TLR2 reporter cells. As illustrated in Fig. S15, the DOCA-HA/OVA@acGM could consistently stimulate TLR2, triggering continuous secretion of SEAP, which could be detected by Quanti-blue solution. In contrast, HA/OVA@acGM rapidly released acGM, and the stimulation declined after day 3. The data suggest that DOCA-HA/OVA@acGM could consistently stimulate TLR2 *in vitro*.

Next, we injected the scaffold vaccine subcutaneously on the left flank of mice and monitored the distribution of scaffold and acGM *in vivo*. As illustrated in Figs. S16A–B, the scaffold was retained in the injection site for a long time, supporting acGM retention and cell infiltration. In addition, the structure of the scaffold was maintained after cell recruitment (Fig. S16C). Also, acGM were mostly retained in the scaffold vaccine, with a very low chance of being released into the body (Fig. S17). However, the signal of acGM in HA/OVA@acGM (with no retention ability) was much lower than that in DOCA-HA/OVA@acGM.

DC maturation and ROS production in the scaffold vaccine at the indicated time points were examined. The number of recruited DCs in the scaffold peaked at day 3 and significantly decreased at 7 days post-injection (Fig. 3A). The number of $CD86^+CD11c^+$ DCs, which was comparable between in DOCA-HA/OVA@acGM and HA/OVA@acGM at day 1 and day 3, sharply decreased by 2/3 in HA/OVA@acGM but maintained steady in DOCA-HA/OVA@acGM until day 7 (Fig. 3B and Fig. S18), suggesting the effect of retention by the interactions between the TLR2 agonist and the DOCA moiety on the scaffold. Also, the maturation of DCs depended on the OVA@acGM, as the scaffold with no OVA@acGM could not induce CD86 expression (Fig. S19). These results suggested the persistent activation of $CD11c^+$ DCs by the retained OVA@acGM in the scaffold.

Then, we determined ROS produced by the activated DCs in the scaffold vaccine and those homing to the lymph nodes (LNs). Consistent with the trend of DC activation, the proportion of $ROS^+CD11c^+$ DCs in the scaffold, which was comparable at day 1 and day 3 between the two groups, was markedly higher in DOCA-HA/OVA@acGM than in HA//OVA@acGM from day 5 (Fig. 3C and Fig. S20). The trend was similar for $ROS^+CD11c^+$ DCs already homing to LNs whereas the fold difference was even larger at day 14 (Fig. 3E and Fig. S21). Notably, the ratio of $ROS^+$ in $CD11c^-$ cells was lower than 2% (dot line, Fig. 3D) and 0.5% (dot line; Fig. 3F) in implants and lymph nodes during immunization, respectively. This was consistent with the fact that TLR2 activation was selective. Importantly, the ratio of $CD8^+/CD4^+$ T cells in the $CD3^+$ lymphocyte subset, as a key indicator of effective adaptive T cell immunotherapy, was significantly elevated in LNs and the spleen after treatment with DOCA-HA/OVA@acGM, compared to HA/OVA@acGM (Fig. 4G-**H, Fig. S22**). **The $CD8^+$ T cell proliferation was attributed to the prolonged and higher cross presentation of DOCA-HA/OVA@acGM (Fig. S23). These data indicated that the retention design effectively sustained ROS production in the DCs recruited into the scaffold that upon activation could migrate from the scaffold to the LNs, successful evoking cellular immune responses.**

### 3.4. In vivo immunotherapeutic efficacy of the scaffold vaccine on tumor growth and metastasis

We investigated the anti-tumor effect of the DOCA-HA/OVA@acGM scaffold vaccine on two aspects in wild-type mice: i) inhibition of tumor growth and ii) prevention of cancer metastasis.

For the first purpose, we implanted the scaffold vaccine subcutaneously into the left flank of the mice 14 days before inoculating melanoma B16-OVA cells ($1 \times 10^6$ per mouse) into the right flank. Then the mice injected with PBS, HA/OVA@acGM (no retention), or OVA@acGM (no scaffold) served as control groups (Fig. 4A). We investigated the levels of IgG, IgG1 and IgG2c to assess the activation of humoral immunity 14 days after immunization. As shown in Fig. 4B, IgG in mice treated with DOCA-HA/OVA@acGM were much higher than in those treated with other formulation, indicating that DOCA-HA/OVA@acGM triggered the strongest humoral response. The profile of IgG2c/IgG1, which is related to Th1-type immune response, was also much higher in mice treated with DOCA-HA/OVA@acGM (Fig. 4C–E), reflected the efficacy of DOCA-HA/OVA@acGM in eventually contributing to tumor inhibition.

Then, the melanoma B16-OVA cells were inoculated, and the anti-tumor efficacy was investigated. Although the two other groups of acGM showed modest anti-tumor performances owing to its established TLR2-activating property, it was only DOCA-HA/OVA@acGM that potently inhibited tumor growth (Fig. 4F, tumor volume; Fig. 4G, gross view). Their contrasting efficacies through this 18-day observation highlighted again the necessity to design acGM-retention scaffold for boosting effective anti-tumor immune responses. During the treatment, no group showed weight fluctuations, suggesting that the mice did not suffer great side effects (Fig. S24). The efficient tumor suppression by DOCA-HA/OVA@acGM led to prolonged survival (Fig. 4H) and substantial apoptosis/necrosis of the tumor cells – as evidenced by and TUNEL (Fig. 4I) staining and histological observation (data not shown) for the tumor samples.

We continued to evaluate the activation of adaptive immunity during this process. Detection of the tumor infiltrating immunocytes by flow cytometry on day 18 revealed that both $CD4^+$ T cells and $CD8^+$ T cells increased significantly more in DOCA-HA/OVA@acGM than in the two other formulations (Fig. 5A), with quantification for $CD4^+$ and $CD8^+$ T cell proportions in Fig. 5B and D, respectively. Meanwhile, the ratio of intratumoral regulatory cells ($T_{reg}$; $CD4^+Foxp3^+$) was markedly reduced (Fig. 5C and Fig. S25). Consistent with the flow cytometry results, immunofluorescent (IF) staining revealed much more tumor-infiltrating $CD8^+$ T cells immunization with DOCA-HA/OVA@acGM than other groups (Fig. 5E), accompanied with the highest proportion of $CD8^+$ T cells that were proliferating ($Ki67^+$; Fig. 5F and Fig. S26A), expressing IFN-γ (Fig. 5G and Fig. S26B), and secreting granzyme B (GranB; Fig. S27 and Fig. S26C). Also, tumor-infiltrating $CD8^+$ T cells which are antigen-specific (OVA-$Tet^+$; Fig. 5H and Fig. S26D) in DOCA-HA/OVA@acGM group were higher than in other groups, suggesting antigen-specific cellular immunity. Consequently, the levels of cytotoxic TNF-α and IFN-γ within the tumors treated with the DOCA-HA/OVA@acGM were also significantly elevated, 3.3 and 8.4-fold higher, respectively, than those of the control group (Fig. S28). Collectively, these results verified the activation of $CD8^+$ T cells by the scaffold vaccine.

For the second purpose, we evaluated the potential of the scaffold vaccine for preventing lung metastasis by triggering immune memory for priming and recognizing "old" antigens. Like the above model, we implanted DOCA-HA/OVA@acGM in parallel with the control groups for 14 days, before setting up a lung metastasis tumor by intravenously infusing B16-OVA tumor cells into the mice. After another 14 days, we investigated lung metastasis (Fig. 6A).

The DOCA-HA/OVA@acGM scaffold demonstrated the highest efficacy in inhibiting metastatic foci formation in the lung (Fig. 6B), with a far lower number of metastasis modules observed than in other groups (quantification, Fig. 6C; histological examination, Fig. 6D), consequently leading to prolonged survival (Fig. 6E). Notably, neither

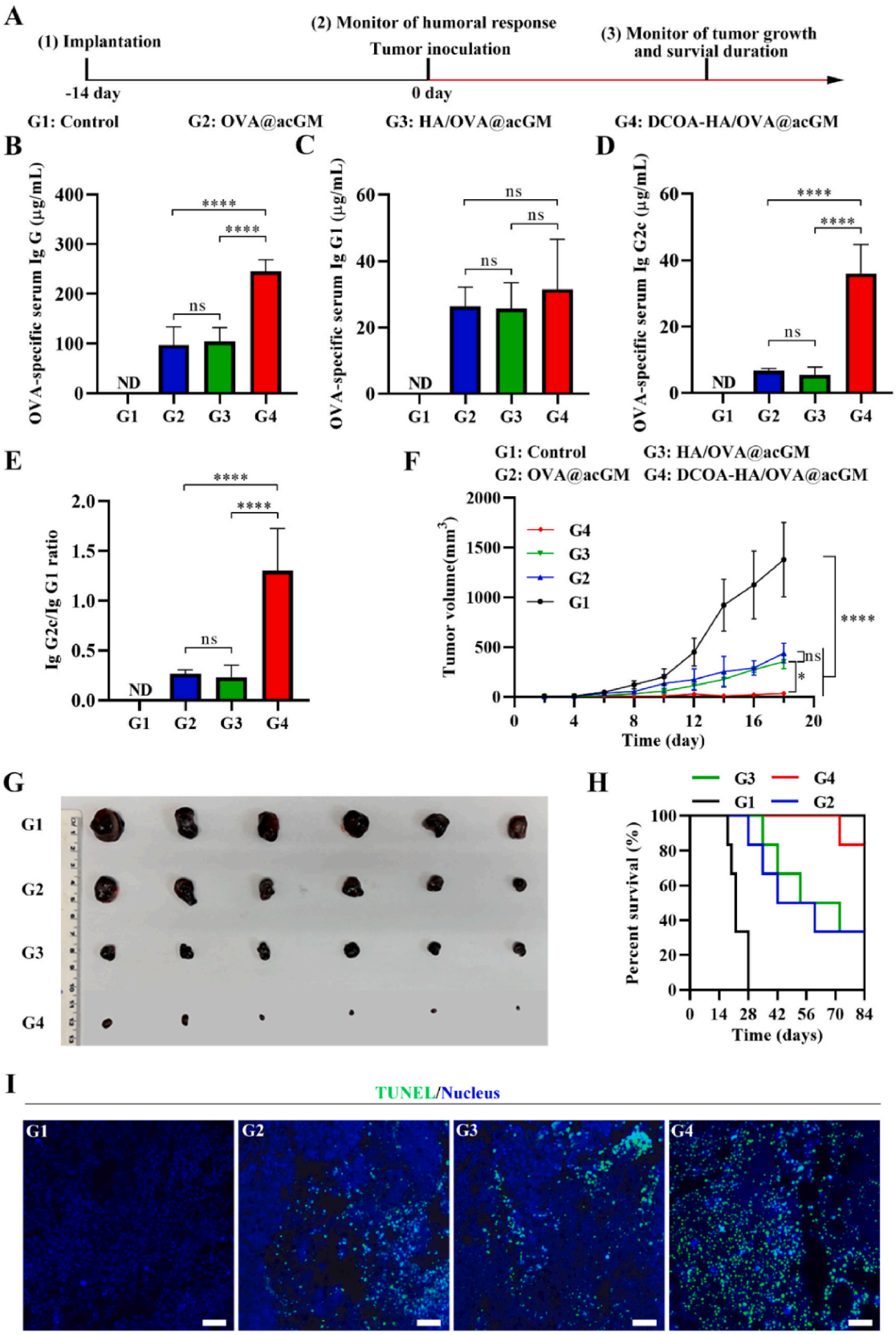


**Fig. 4.** The OVA-laden scaffold vaccine inhibited the growth of B16-OVA tumors subcutaneously localized in wide-type mice. (A) Therapeutic schedule for scaffold vaccine. Schematic of the experiment design. **(B–D)** Levels of anti-OVA IgG (**B**), IgG1 (**C**), and IgG2c (**D**) antibodies in serum were determined. **(E)** The ratio of IgG2c to IgG1. **(F)** The tumor growth curve of B16-OVA subcutaneous model. **(G)** Photographs of the tumors at the end of treatment. **(H)** Survival percentage of the B16-OVA tumor-bearing C57BL/6J mice receiving different treatments. **(I)** TUNEL staining of the tumor sections examined at the end of antitumor treatment. Scale bar: 100 μm. $n \geq 5$, values represent means ± standard deviation. Statistical significance was calculated by one-way ANOVA using the Tukey posttest. ns: no significance; *$p < 0.05$, **$p < 0.01$, ***$p < 0.001$, ****$p < 0.0001$.

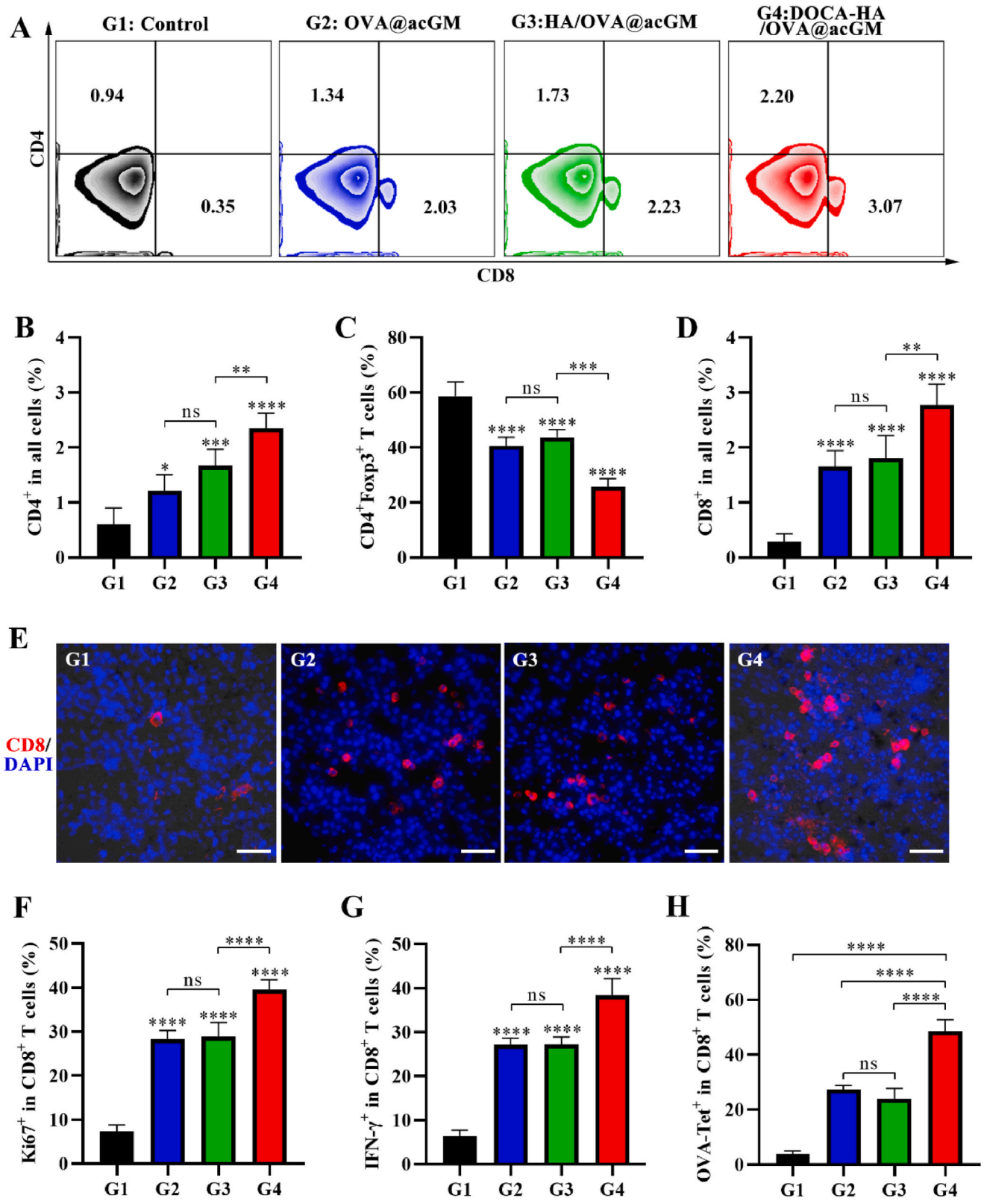


**Fig. 5. The OVA-laden scaffold vaccine generated robust CD8$^+$ T cell-mediated immune responses against B16-OVA tumors subcutaneously localized in wild-type mice. (A)** Representative flow cytometry analysis of the tumor-infiltrated T cells. **(B)** Quantitation of the percentage of CD4$^+$ T cells in the tumor. **(C)** Quantitative analysis of Treg cells in tumor tissues. **(D)** Quantitation of the percentage of CD8$^+$ T cells in the tumor. **(E)** CD8$^+$ T cell staining of the tumor sections examined at the end of anti-tumor treatment. Scale bar: 50 μm. **(F)** Proportion of Ki67$^+$ within CD8$^+$ T cells. **(G)** Proportion of IFN-γ within CD8$^+$ T cells. **(H)** Proportion of OVA-Tet$^+$ within CD8$^+$ T cells. G1: Control; G2: OVA@acGM; G3: HA/OVA@acGM; G4: DOCA-HA/OVA@acGM. $n \geq 5$, values represent means ± standard deviation. Statistical significance was calculated by one-way ANOVA using the Tukey posttest. ns: no significance; *$p < 0.05$, **$p < 0.01$, ***$p < 0.001$, ****$p < 0.0001$.

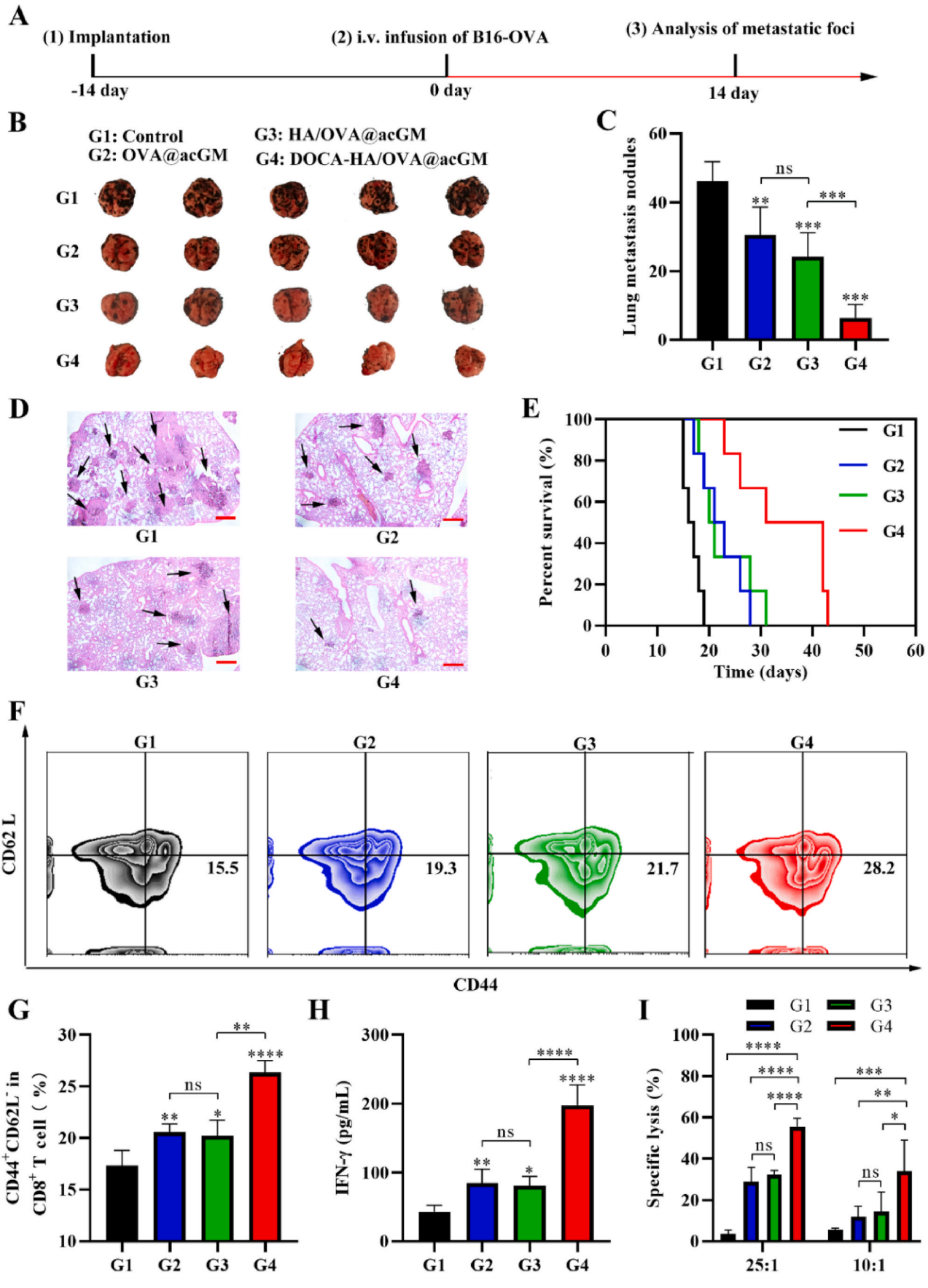


*(caption on next page)*

**Fig. 6. The scaffold vaccine generated lasting immune memory against metastatic lung cancer in wild-type mice.** Scaffold vaccine prevent metastasis *via* long term immune memory effects. **(A)** Therapeutic schedule for scaffold vaccine to inhibit tumor metastasis. **(B)** Representative photographs of lung tissues. **(C)** Quantification of pulmonary metastasis nodes on mice pre-vaccinated with OVA@acGM, HA/OVA@acGM or DOCA-HA/OVA@acGM. **(D)** H&E staining of the lung tissue collected at day 14. Scale bars: 250 μm. **I** Survival percentage of C57BL/6J mice i.v. infused with B16-OVA cells after vaccination. **(F)** Flow cytometry plots of effector memory T cells in the spleen examined at the same day for i.v. infusion of the B16-OVA cells. **(G)** Proportions of effector memory T cells in the spleen examined at the same day for i.v. infusion of the B16-OVA cells. **(H)** The IFN-γ production in splenocyte supernatant after 3-day restimulation with $OVA_{257-264}$ measured by ELISA. G1: Control; G2: OVA@acGM; G3: HA/OVA@acGM; G4: DOCA-HA/OVA@acGM. **(I)** The tumor cells lysis by splenocyte restimulated with $OVA_{257-264}$. G1: Control; G2: OVA@acGM; G3: HA/OVA@acGM; G4: DOCA-HA/OVA@acGM. $n = 5$, values represent means ± standard deviation. Statistical significance was calculated by one-way ANOVA using the Tukey posttest. Ns: no significance; $^{*}p < 0.05$, $^{**}p < 0.01$, $^{***}p < 0.001$, $^{****}p < 0.0001$.

OVA@acGM (no scaffold) nor HA/OVA@acGM (no retention) could effectively prevent lung metastasis. The foci number in these treatments remained as high as 60–70% of that in the blank control – especially, 3.78-fold higher in the HA/OVA@acGM group than in the DOCA-HA/OVA@acGM – which further stressed the importance of acGM retention in our scaffold design.

To understand the mechanism underlying this anti-metastasis effect of the scaffold vaccine, we examined the effector memory ($CD8^+CD44^+CD62L^-$) T cells in the spleen using flow cytometry upon the infusion of B16-OVA cells. Among the groups, only DOCA-HA/OVA@acGM vaccination significantly increased the frequency of effector memory T cells in the spleen (1.52-time that of control) (Fig. 6F and **G**). Particularly, upon stimulation with the $OVA_{257-264}$ peptide, the splenic cells from mice immunized with DOCA-HA/OVA@acGM secreted significantly more IFN-γ (4.61 time that of control) – in contrast to the other two samples that barely induced ~ 2 times secretion – providing evidence that the scaffold vaccine could effectively induce antigen-specific adaptive immunity (Fig. 6H). To further assess whether the activated immune cells were enough to recognize and kill antigen-bearing target cells, we evaluated OVA-specific cytotoxic T lymphocyte activity. As shown in Fig. 6I, DOCA-HA/OVA@acGM caused a significantly higher percentage of target cell lysis than other groups. OVA@acGM and HA/OVA@acGM were comparable in OVA-specific lysis and higher than the control group. These results suggested that the scaffold vaccine displayed high efficacy to inhibit lung metastasis.

In addition, the treatment with the scaffold vaccines has no significant influences on the heart, liver, spleen, lung, and kidney as the main organs of mice, supporting the safety of our devised polysaccharide-based material (Fig. S29).

### 3.5. *In vivo immunotherapeutic efficacy of the scaffold vaccine against spontaneous colorectal tumor*

Finally, we tested the effects of the DOCA-HA scaffold for loading TSA@acGM to prevent spontaneous tumor development in transgenic $APC^{min/+}$ mice, which are remarkably susceptible to spontaneous intestinal adenoma and a commonly used animal model for cancer research. Specifically, the tumor cells from the tumor-burden mice cells were lysed and formulated into DOCA-HA/TSA@acGM, which were injected to immunize the normal $Apc^{min+}$ mice (Fig. 7A).

To verify the efficiency of DOCA-HA/TSA@acGM, we harvested the splenic $CD8^+$ T cells and restimulated them with TSA, and the secreted IFN-γ by $CD8^+$ T cells was determined. As shown in Fig. 7B, IFN-γ in the DOCA-HA/TSA@acGM group was much higher (9.63 times, *versus* control), suggesting the induction of antigen-specific immune response. As shown in Fig. 7C and **D**, DOCA-HA@TSA greatly reduced the size and number of the tumors in the colon. The TUNEL staining of tumor tissues (Fig. 7E) showed that the maximal apoptosis of the tumor cells was observed in the mice treated with DOCA-HA/TSA@acGM compared with control group, which could be attributed to $CD8^+$ T cell infiltration and activation (Fig. 7F and **G**). The percentage of $Ki67^+$ within $CD8^+$ T cells in tumor of mice treated with DOCA-HA/TSA@acGM was 1.55-fold of control, indicating that the $CD8^+$ T cells underwent proliferation (Fig. 7G). The proliferating $CD8^+$ T cells were the main source of IFN-γ and Granzyme B with direct toxicity to the tumor cells (Fig. 7H and I). These results suggested that DOCA-HA/TSA@acGM could reduce the progression of spontaneous tumor in $Apc^{Min/+}$ mouse model.

## 4. Discussion

A long-standing challenge for cancer immunotherapy is the effective presentation of tumor antigens to cytotoxic $CD8^+$ T cells, which are the most potent effector lymphocytes for orchestrating desirable anti-tumor immune responses. The critical hurdle to achieving this goal is to ensure efficient cross-presentation – DCs present the extrinsic tumor antigens through surface MHC-I to $CD8^+$ T cells. In this study, we have developed a 3D scaffold vaccine aimed at overcoming this hurdle. Its most prominent function is the retention-and-release of an immunoactive glycan to exert sustained TLR2 activation, which creates optimal kinetics for intracellular ROS production (another novel finding from the present study) and, eventually, induces effective antigen cross-presentation.

Scaffold vaccines possess special advantages for cancer immunotherapy, as they create the space for enriching abundant immune cells [27,28] and flexibility to adjust the release of incorporated molecules (e.g. antigens, adjuvants, or cytokines), for accurate stimulation of immune responses [29] including robust anti-tumor responses. The design of these scaffolds considers the physical and chemical properties of macromolecules from the beginning to control their behaviors, as their molecular weight [30] and charge properties [29] affect the release behavior of incorporated molecules. For instance, small molecular drugs rely on carriers (particles or scaffolds) to exert their spatiotemporal effects [31] and avoid rapid diffusion in the body [32]. Bioactive macromolecules, especially those assembled into particles, were often released by diffusion over desired time frames in weakly interacting particles/scaffold systems [33]. The release of mesoporous silicon nanoparticles from 3D hydrogel scaffolds can easily be modulated over times from days to weeks through tuning of electrostatic nanoparticle – polymer and nanoparticle – nanoparticle interactions [34], and the strength of such nanoparticle-hydrogel binding is tunable [35]. In this work, hydrophobic interaction was exploited to control the retention of hydrophobic molecules for the first time. Briefly, we modified hydrophobic moieties, e.g., C6, C14, or DOCA, to the hydrophilic HA polysaccharide chains, endowing HA with the ability to interact with acGM – which, interestingly, is also composed of hydrophobic acetyl moieties on hydrophilic glucomannan polysaccharide frameworks. This hydrophobic interaction formed the basis for the retention-release function. On top of this interaction, we further employed PEG-8DBCO to crosslink the scaffold with click chemistry triggering. This scaffold significantly retained the hydrophobic acGM. Our findings may provide new strategies to control and tune the behaviors of hydrophobic macromolecules.

In addition, biomaterials with inherent properties are often utilized for encapsulating and delivering bioactive molecules, of which the release kinetics can be controlled by various factors, including the type of scaffold material, encapsulation method, and formulation design [36,37]. In our work, the 3D hydrogel formed by click chemistry can encapsulate hydrophilic GM-CSF proteins evenly dispersed in its porous structure and allows for their sustained release. The antigenic proteins (e.g. OVA and TSA) were encapsulated into the acGM through double emulsion. The release rate of OVA@acGM is an important consideration as it affects the duration and intensity of the immune response generated by the scaffold vaccine. Explosive or rapid release led to inefficient

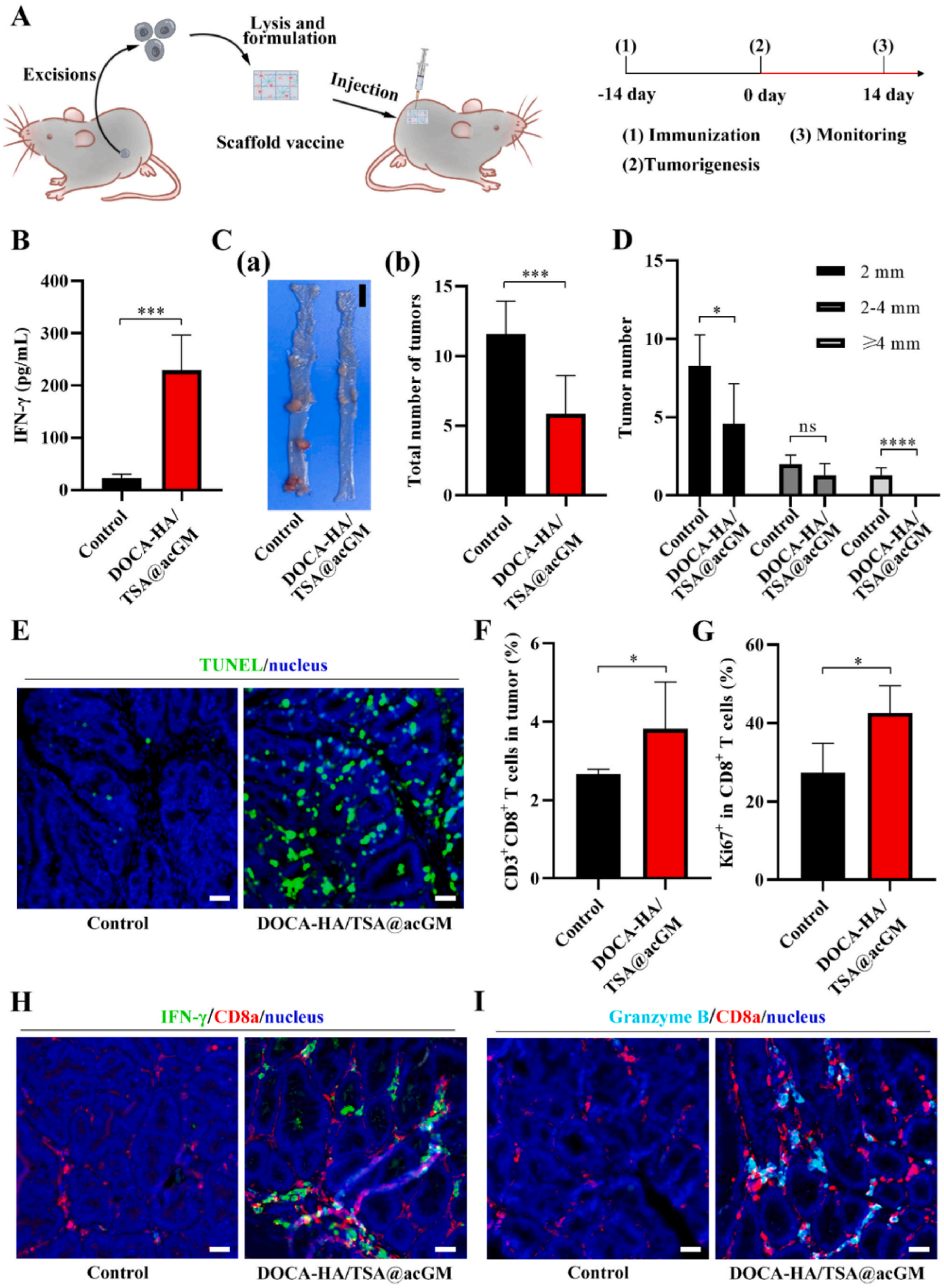


*(caption on next page)*

**Fig. 7. The TSA-laden scaffold vaccine generated robust anti-tumor responses against spontaneous colorectal tumor in transgenic $Apc^{min/+}$ mice.** **(A)** Schematic of scaffold vaccine to prevent the progression of spontaneous colorectal tumor. **(B)** The IFN-γ production in supernatant of $CD8^+$ T cells harvested from immunized mice and restimulated with TSA for 3 days. **(C)** Photographs of the tumors at the end of treatment **(a)** and total number of tumors in colon **(b)**. **(D)** Number of tumors in different size range. **(E)** TUNEL staining of tumor in the colon after DOCA-HA/TSA@acGM treatment. Scale bar: 50 μm. **(F)** Proportion of $CD8^+$ within $CD3^+$ T cells. **(G)** Proportion of Ki67 within $CD8^+$ T cells. **(H)** Immunostaining in the tumor at day 14 showing $CD8^+$ T cells (Red), and IFN-γ (green). Scale bar: 50 μm. **(I)** Immunostaining in the tumor at day 14 showing $CD8^+$ T cells (Red), and Granzyme B (Cyan). Scale bar: 50 μm. $n \geq 5$, values represent means ± standard deviation. Statistical significance was calculated by student's t-test. ns: no significance; $^*p < 0.05$, $^{**}p < 0.01$, $^{***}p < 0.001$, $^{****}p < 0.0001$.

recruitment and activation of DCs. In our work, cell recruitment peaked at day 3 and day 5, when OVA@acGM was still retained in DOCA-HA/OVA@acGM, facilitating DC maturation and subsequent cross-presentation.

We devised the strategy of activating TLR2 with acGM for prolonged intracellular ROS, based on clear rationale and safety considerations. First, we chose to regulate an intrinsic and well-established biological pathway to stimulate ROS production for higher controllability – hence choosing cell-surface TLRs over direct manipulation of intracellular machinery. In the past decades, a series of studies have illustrated this biological process, including the crucial role of ROS in regulating cross-presentation [8,23], the process how receptor-mediated ROS production is coupled with NOX isozymes (e.g., NOX2, NOX4) in phagocytic cells [22], as well as the association between the C-terminal region of NOX2 and the TIR domain of TLR2 initialize the ROS production [20]. Second, we innovatively identified the optimal kinetics of ROS production for antigen presentation, which was hardly investigated before. Based on our findings that confirmed the necessity of sustained TLR2 activation, we designed the 3D scaffold vaccine for retention-and-release of the agonist, so as to achieve the kinetics of ROS production and meanwhile avoid repeated injection of the agonist. Third, we employed the large-molecule acGM instead of small-molecule TLR2 agonists, as acGM is comparable in efficacy to commercial TLR2 agonist while possessing the advantage of encapsulating antigens, as demonstrated in our previous study [25]; in addition, the release behavior of acGM is more controllable, as small molecular could easily diffuse from the scaffold. Our serial data from three *in vivo* models confirmed that the system could potently trigger anti-tumor $CD8^+$ T cell responses.

We first tested OVA as a model antigen to verify that ROS kinetics could be modulated for antigen cross-presentation, thus inducing robust anti-tumor immunity. Since the tumor lysate contains the whole array of mutated epitopes for parallel presentation to both $CD8^+$ and $CD4^+$ T cells, which reduces the likelihood of tumor escape [38,39], we used whole tumor lysate from a spontaneous, colorectal cancer model to broaden the application of this strategy. As demonstrated above, the scaffold vaccine incorporated with whole tumor lysates exhibited encouraging anti-tumor efficacy against spontaneous colorectal cancer. The ability to stimulate the immune response is one clear advantage of our scaffold vaccine. Sustained TLR2 activation in DCs eventually led to increased production of the IgG2c antibody, a manifestation of effective $T_H1$ response [40]. Particularly, the awakening of $CD8^+$ T cell-mediated responses was evident in both types of immunized mice (C57 and $Apc^{Min/+}$ mice), which had significantly activated $CD8^+$ T cells (IFN-$\gamma^+$ and $GramB^+$) and proliferative ($Ki67^+$), showing the potential of this scaffold as a generic platform for tumor vaccine to induce robust $CD8^+$ T cell-mediated adaptive immunity for different antigens (OVA or TSA). In future, patient-specific antigens should be obtained from autologous tumor cells of individual patients should be tested, so as to evaluate the translational potential of this scaffold vaccine for personalized cancer immunotherapy.

## 5. Conclusion

In this study, we report a 3D, injectable scaffold vaccine for efficient stimulation of antigen cross-presentation that triggered robust $CD8^+$ T cell-mediated immune responses. As the first significant novelty, we have uncovered the effect of the kinetics of intracellular ROS production on the type of antigen (cross-)presentation, which serves as a fundamental mechanism for designing vaccines or adjuvants but was barely known. Based on this vital discovery, we designed a polysaccharide framework decorated with optimized hydrophobic moieties to form tunable interactions with an amphiphilic glycan – also an established TLR2 agonist. Upon subcutaneous injection of the complex, it formed a 3D porous scaffold to achieve retention and release of the agonist, achieving sustained TLR2 activation in the recruited dendritic cells (DCs). Our comprehensive tests in three models in two mice – localized and metastatic lung tumors in C57 mice and spontaneous colorectal cancer in transgenic $Apc^{Min/+}$ mice demonstrated that this vaccine system generated potent and lasting anti-tumor immune responses. The advantages that this system requires no additional adjuvants or external triggering system, together with the satisfactory *in vivo* safety data, further highlight the translational potential of this innovative vaccine for future design of cancer vaccination therapies.

## Ethics approval

All experimental designs and protocols involving animals were approved by the by the University of Macau Animal Research Ethics Committee (No. UMARE-007-2022) and Nanjing University Animal Research Ethics Committee (No. IACUC-2306010). The authors declare that all experiments involving animals were in compliance with relevant ethical regulations.

## CRediT authorship contribution statement

**Daping Xie:** Writing – original draft, Methodology, Investigation, Data curation, Conceptualization. **Congwei Han:** Methodology, Investigation. **Chonghao Chen:** Investigation. **Zhencheng Liao:** Visualization, Methodology. **Senio Campos de Souza:** Writing – original draft. **Yiming Niu:** Methodology. **João F. Mano:** Methodology. **Lei Dong:** Supervision, Resources, Funding acquisition. **Chunming Wang:** Writing – original draft, Supervision, Funding acquisition, Conceptualization.

## Declaration of competing interest

The authors declare that they have no known competing financial interests or personal relationships that could have appeared to influence the work reported in this paper.

## Acknowledgements

We thank Ms Zijun Zheng and Ms Jiaxi Chen for their technical help in biological experiments. This study was financially supported by the Science and Technology Development Fund, Macao SAR (FDCT, No. 0001/2021/AKP, 0024/2023/AFJ, 0060/2020/AGJ, and 005/2023/SKL), the National Natural Science Foundation of China (NSFC, No. 31961160701, 32022088, 31971309, 32001069, 32230056, and 32000936), the Natural Science Foundation of Jiangsu Province (BK20200318), and the University of Macau (MYRG-GRG2023-00136-ICMS-UMDF and MYRG2022-00100-ICMS). JFM acknowledges the support from the project CICECO-Aveiro Institute of Materials, UIDB/50011/2020, UIDP/50011/2020 & LA/P/0006/2020, financed by national funds through the FCT/MEC (PIDDAC).

## Appendix A. Supplementary data

Supplementary data to this article can be found online at https://doi.org/10.1016/j.bioactmat.2024.03.035.

## References


[1] J. Liu, M. Fu, M. Wang, D. Wan, Y. Wei, X. Wei, Cancer vaccines as promising immuno-therapeutics: platforms and current progress, J. Hematol. Oncol. 15 (1) (2022) 28, https://doi.org/10.1186/s13045-022-01247-x.

[2] M.J. Lin, J. Svensson-Arvelund, G.S. Lubitz, A. Marabelle, I. Melero, B.D. Brown, J. D. Brody, Cancer vaccines: the next immunotherapy frontier, Nat. Cancer 3 (8) (2022) 911–926, https://doi.org/10.1038/s43018-022-00418-6.

[3] J. Chen, H. Zhang, L. Zhou, Y. Hu, M. Li, Y. He, Y. Li, Enhancing the efficacy of tumor vaccines based on immune evasion mechanisms, Front. Oncol. 10 (2020) 584367, https://doi.org/10.3389/fonc.2020.584367.

[4] O.J. Finn, Cancer vaccines: between the idea and the reality, Nat. Rev. Immunol. 3 (8) (2003) 630–641, https://doi.org/10.1038/nri1150.

[5] C.M. Fehres, W.W.J. Unger, J.J. Garcia-Vallejo, Y. van Kooyk, Understanding the biology of antigen cross-presentation for the design of vaccines against cancer, Front. Immunol. 5 (2014), https://doi.org/10.3389/fimmu.2014.00149.

[6] H. Shen, A.L. Ackerman, V. Cody, A. Giodini, E.R. Hinson, P. Cresswell, R. L. Edelson, W.M. Saltzman, D.J. Hanlon, Enhanced and prolonged cross-presentation following endosomal escape of exogenous antigens encapsulated in biodegradable nanoparticles, Immunology 117 (1) (2006) 78–88, https://doi.org/10.1111/j.1365-2567.2005.02268.x.

[7] A. Savina, C. Jancic, S. Hugues, P. Guermonprez, P. Vargas, I.C. Moura, A.-M. Lennon-Duménil, M.C. Seabra, G. Raposo, S. Amigorena, NOX2 controls phagosomal pH to regulate antigen processing during crosspresentation by dendritic cells, Cell 126 (1) (2006) 205–218, https://doi.org/10.1016/j.cell.2006.05.035.

[8] I. Dingjan, D.R.J. Verboogen, L.M. Paardekooper, N.H. Revelo, S.P. Sittig, L. J. Visser, G.F.v. Mollard, S.S.V. Henriet, C.G. Figdor, M. ter Beest, G. van den Bogaart, Lipid peroxidation causes endosomal antigen release for cross-presentation, Sci. Rep. 6 (1) (2016) 22064, https://doi.org/10.1038/srep22064.

[9] N. Salame, J.-P. Bikorimana, N. El-Hachem, W. Saad, M. Kurdi, J. Zhao, N. Eliopoulos, R. Shammaa, M. Rafei, UM171A-induced ROS promote antigen cross-presentation of immunogenic peptides by bone marrow-derived mesenchymal stromal cells, Stem Cell Res. Ther. 13 (1) (2022) 16, https://doi.org/10.1186/s13287-021-02693-z.

[10] T. Zaidieh, J.R. Smith, K.E. Ball, Q. An, ROS as a novel indicator to predict anticancer drug efficacy, BMC Cancer 19 (1) (2019) 1224, https://doi.org/10.1186/s12885-019-6438-y.

[11] G. Chong, R. Su, J. Gu, Y. Yang, T. Zhang, J. Zang, Y. Zhao, X. Zheng, Y. Liu, S. Ruan, R. He, W. Yin, Y. Li, H. Dong, Y. Li, Catalytic nanovaccine for cancer immunotherapy: a NADPH oxidase-inspired Fe-polyphenol network nanovaccine for enhanced antigen cross-presentation, Chem. Eng. J. 435 (2022) 134993, https://doi.org/10.1016/j.cej.2022.134993.

[12] D. Mao, F. Hu, Z. Yi, S. Xu, S. Yan, Z. Luo, W. Wu, Z. Wang, D. Kong, X. Liu, B. Liu, AIEgen-coupled upconversion nanoparticles eradicate solid tumors through dual-mode ROS activation, Sci. Adv. 6 (26) (2020) eabb2712, https://doi.org/10.1126/sciadv.abb2712.

[13] Z. Yu, Q. Li, J. Wang, Y. Yu, Y. Wang, Q. Zhou, P. Li, Reactive oxygen species-related nanoparticle toxicity in the biomedical field, Nanoscale Res. Lett. 15 (1) (2020) 115, https://doi.org/10.1186/s11671-020-03344-7.

[14] N.-L. Pham, V. Badovinac, J. Harty, Differential role of "signal 3" inflammatory cytokines in regulating CD8 T cell expansion and differentiation in vivo, Front. Immunol. 2 (2011), https://doi.org/10.3389/fimmu.2011.00004.

[15] S. Fuse, W. Zhang, E.J. Usherwood, Control of memory CD8+ T cell differentiation by CD80/CD86-CD28 costimulation and restoration by IL-2 during the recall Response1, J. Immunol. 180 (2) (2008) 1148–1157, https://doi.org/10.4049/jimmunol.180.2.1148.

[16] S.W. Van Gool, P. Vandenberghe, M.d. Boer, J.L. Ceuppens CD80, CD86 and CD40 provide accessory signals in a multiple-step T-cell activation model, Immunol. Rev. 153 (1) (1996) 47–83, https://doi.org/10.1111/j.1600-065X.1996.tb00920.x.

[17] A. Mauriello, C. Manolio, B. Cavalluzzo, A. Avallone, M. Borrelli, A. Morabito, E. Iovine, A. Chambery, R. Russo, M.L. Tornesello, F.M. Buonaguro, M. Tagliamonte, L. Buonaguro, Immunological effects of adjuvants in subsets of antigen presenting cells of cancer patients undergoing chemotherapy, J. Transl. Med. 18 (1) (2020) 34, https://doi.org/10.1186/s12967-020-02218-x.

[18] L.E. Feinendegen, Reactive oxygen species in cell responses to toxic agents, Hum. Exp. Toxicol. 21 (2) (2002) 85–90, https://doi.org/10.1191/0960327102ht216oa.

[19] T. Kawai, S. Akira, The roles of TLRs, RLRs and NLRs in pathogen recognition, Int. Immunol. 21 (4) (2009) 317–337, https://doi.org/10.1093/intimm/dxp017.

[20] C.S. Yang, D.M. Shin, K.H. Kim, Z.W. Lee, C.H. Lee, S.G. Park, Y.S. Bae, E.K. Jo, NADPH oxidase 2 interaction with TLR2 is required for efficient innate immune responses to mycobacteria via cathelicidin expression, J. Immunol. 182 (6) (2009) 3696–3705, https://doi.org/10.4049/jimmunol.0802217.

[21] M.M. Romero, J.I. Basile, L. Corra Feo, B. López, V. Ritacco, M. Alemán, Reactive oxygen species production by human dendritic cells involves TLR2 and dectin-1 and is essential for efficient immune response against Mycobacteria, Cell Microbiol. 18 (6) (2016) 875–886, https://doi.org/10.1111/cmi.12562.

[22] H.S. Park, H.Y. Jung, E.Y. Park, J. Kim, W.J. Lee, Y.S. Bae, Cutting edge: direct interaction of TLR4 with NAD(P)H oxidase 4 isozyme is essential for lipopolysaccharide-induced production of reactive oxygen species and activation of NF-κB1, J. Immunol. 173 (6) (2004) 3589–3593, https://doi.org/10.4049/jimmunol.173.6.3589%JTheJournalofImmunology.

[23] M. Oberkampf, C. Guillerey, J. Mouriès, P. Rosenbaum, C. Fayolle, A. Bobard, A. Savina, E. Ogier-Denis, J. Enninga, S. Amigorena, C. Leclerc, G. Dadaglio, Mitochondrial reactive oxygen species regulate the induction of CD8+ T cells by plasmacytoid dendritic cells, Nat. Commun. 9 (1) (2018) 2241, https://doi.org/10.1038/s41467-018-04686-8.

[24] C.M.C. Andrés, J.M. Pérez de la Lastra, C.A. Juan, F.J. Plou, E. Pérez-Lebeña, The role of reactive species on innate immunity, Vaccines 10 (10) (2022) 1735, https://doi.org/10.3390/vaccines10101735.

[25] D. Xie, Y. Niu, R. Mu, S. Campos de Souza, X. Yin, L. Dong, C. Wang, A toll-like receptor-activating, self-adjuvant glycan nanocarrier, Front. Chem. 10 (2022), https://doi.org/10.3389/fchem.2022.864206.

[26] Y. Feng, R. Mu, Z. Wang, P. Xing, J. Zhang, L. Dong, C. Wang, A toll-like receptor agonist mimicking microbial signal to generate tumor-suppressive macrophages, Nat. Commun. 10 (1) (2019) 2272, https://doi.org/10.1038/s41467-019-10354-2.

[27] Y. Zhang, J. Xu, Z. Fei, H. Dai, Q. Fan, Q. Yang, Y. Chen, B. Wang, C. Wang, 3D printing scaffold vaccine for antitumor immunity, Adv. Mater. 33 (48) (2021) 2106768, https://doi.org/10.1002/adma.202106768.

[28] O.A. Ali, N. Huebsch, L. Cao, G. Dranoff, D.J. Mooney, Infection-mimicking materials to program dendritic cells in situ, Nat. Mater. 8 (2) (2009) 151–158, https://doi.org/10.1038/nmat2357.

[29] A.J. Najibi, M.O. Dellacherie, T.-Y. Shih, E.J. Doherty, D.A. White, T. Bauleth-Ramos, A.G. Stafford, J.C. Weaver, C.D. Yeager, B.T. Seiler, M. Pezone, A.W. Li, B. Sarmento, H.A. Santos, D.J. Mooney, L. Gu, Scaffold vaccines for generating robust and tunable antibody responses, Adv. Funct. Mater. 32 (16) (2022) 2110905, https://doi.org/10.1002/adfm.202110905.

[30] C. Wang, J. Wang, X. Zhang, S. Yu, D. Wen, Q. Hu, Y. Ye, H. Bomba, X. Hu, Z. Liu, G. Dotti, Z. Gu, In situ formed reactive oxygen species–responsive scaffold with gemcitabine and checkpoint inhibitor for combination therapy, Sci. Transl. Med. 10 (429) (2018) eaan3682, https://doi.org/10.1126/scitranslmed.aan3682.

[31] V. Ogay, E.A. Mun, G. Kudaibergen, M. Baidarbekov, K. Kassymbek, Z. Zharkinbekov, A. Saparov, Progress and prospects of polymer-based drug delivery systems for bone tissue regeneration, Polymers 12 (12) (2020) 2881, https://doi.org/10.3390/polym12122881.

[32] J. Wagner, D. Gößl, N. Ustyanovska, M. Xiong, D. Hauser, O. Zhuzhgova, S. Hočevar, B. Taskoparan, L. Poller, S. Datz, H. Engelke, Y. Daali, T. Bein, C. Bourquin, Mesoporous silica nanoparticles as pH-responsive carrier for the immune-activating drug resiquimod enhance the local immune response in mice, ACS Nano 15 (3) (2021) 4450–4466, https://doi.org/10.1021/acsnano.0c08384.

[33] J.T. Kalathi, U. Yamamoto, K.S. Schweizer, G.S. Grest, S.K. Kumar, Nanoparticle diffusion in polymer nanocomposites, Phys. Rev. Lett. 112 (10) (2014) 108301, https://doi.org/10.1103/PhysRevLett.112.108301.

[34] B. Baumann, T. Jungst, S. Stichler, S. Feineis, O. Wiltschka, M. Kuhlmann, M. Lindén, J. Groll, Control of nanoparticle release kinetics from 3D printed hydrogel scaffolds, Angew. Chem. Int. Ed. 56 (16) (2017) 4623–4628, https://doi.org/10.1002/anie.201700153.

[35] E.A. Appel, M.W. Tibbitt, M.J. Webber, B.A. Mattix, O. Veiseh, R. Langer, Self-assembled hydrogels utilizing polymer–nanoparticle interactions, Nat. Commun. 6 (1) (2015) 6295, https://doi.org/10.1038/ncomms7295.

[36] S.-H. Lee, H. Shin, Matrices and scaffolds for delivery of bioactive molecules in bone and cartilage tissue engineering, Adv. Drug Deliv. Rev. 59 (4) (2007) 339–359, https://doi.org/10.1016/j.addr.2007.03.016.

[37] K. Adu-Berchie, D.J. Mooney, Biomaterials as local niches for immunomodulation, Acc. Chem. Res. 53 (9) (2020) 1749–1760, https://doi.org/10.1021/acs.accounts.0c00341.

[38] C.L.-L. Chiang, F. Benencia, G. Coukos, Whole tumor antigen vaccines, Semin. Immunol. 22 (3) (2010) 132–143, https://doi.org/10.1016/j.smim.2010.02.004.

[39] T. Wang, D. Wang, H. Yu, B. Feng, F. Zhou, H. Zhang, L. Zhou, S. Jiao, Y. Li, A cancer vaccine-mediated postoperative immunotherapy for recurrent and metastatic tumors, Nat. Commun. 9 (1) (2018) 1532, https://doi.org/10.1038/s41467-018-03915-4.

[40] J. Kim, W.A. Li, Y. Choi, S.A. Lewin, C.S. Verbeke, G. Dranoff, D.J. Mooney, Injectable, spontaneously assembling, inorganic scaffolds modulate immune cells in vivo and increase vaccine efficacy, Nat. Biotechnol. 33 (1) (2015) 64–72, https://doi.org/10.1038/nbt.3071.